Received: 17 November 2021 | Revised: 7 February 2022 | Accepted: 17 February 2022

DOI: 10.1002/pro.4290

FULL-LENGTH PAPER

THE PROTEIN SOCIETY WILEY

Characterization of the glutathione-dependent reduction of the peroxiredoxin 5 homolog PfAOP from *Plasmodium falciparum*

Robin Schumann | **Lukas Lang** | **Marcel Deponte**

Faculty of Chemistry, TU Kaiserslautern, Kaiserslautern, Germany

Correspondence
Marcel Deponte, Faculty of Chemistry/Biochemistry, TU Kaiserslautern, D-67663 Kaiserslautern, Germany.
Email: deponte@chemie.uni-kl.de

Funding information
Deutsche Forschungsgemeinschaft, Grant/Award Number: DE 1431/8-2

Review Editor: John Kuriyan

Abstract

Peroxiredoxins use a variety of thiols to rapidly reduce hydroperoxides and peroxynitrite. While the oxidation kinetics of peroxiredoxins have been studied in great detail, enzyme-specific differences regarding peroxiredoxin reduction and the overall rate-limiting step under physiological conditions often remain to be deciphered. The 1-Cys peroxiredoxin 5 homolog PfAOP from the malaria parasite *Plasmodium falciparum* is an established model enzyme for glutathione/glutaredoxin-dependent peroxiredoxins. Here, we reconstituted the catalytic cycle of PfAOP *in vitro* and analyzed the reaction between oxidized PfAOP and reduced glutathione (GSH) using molecular docking and stopped-flow measurements. Molecular docking revealed that oxidized PfAOP has to adopt a locally unfolded conformation to react with GSH. Furthermore, we determined a second-order rate constant of 6×10^5 M^{-1} s^{-1} at 25°C and thermodynamic activation parameters $\Delta H^{\ddagger}$, $\Delta S^{\ddagger}$, and $\Delta G^{\ddagger}$ of 39.8 kJ/mol, −0.8 J/mol, and 40.0 kJ/mol, respectively. The gain-of-function mutant $PfAOP^{L109M}$ had almost identical reaction parameters. Taking into account physiological hydroperoxide and GSH concentrations, we suggest (a) that the reaction between oxidized PfAOP and GSH might be even faster than the formation of the sulfenic acid *in vivo*, and (b) that conformational changes are likely rate limiting for PfAOP catalysis. In summary, we characterized and quantified the reaction between GSH and the model enzyme PfAOP, thus providing detailed insights regarding the reactivity of its sulfenic acid and the versatile chemistry of peroxiredoxins.

KEYWORDS

1-Cys peroxiredoxin, enzyme mechanism, glutathione, peroxiredoxin 5, peroxiredoxin catalysis, *Plasmodium falciparum*, stopped-flow kinetics, sulfenic acid

Robin Schumann and Lukas Lang contributed equally to this work.

1 | INTRODUCTION

Peroxiredoxins are highly versatile thiol-dependent hydroperoxidases that can also act as redox sensors and chaperones.[1–4] In addition to their subcellular localization, members of the peroxiredoxin family are grouped into three different mechanistic and six major structural subfamilies.[1,5–7] The human malaria parasite *Plasmodium falciparum* has four peroxiredoxin isoforms,[8] one of which, termed antioxidant protein (PfAOP), is a member of the peroxiredoxin 5 subfamily.[9] PfAOP is dually localized in the cytosol and the apicoplast of *P. falciparum*.[10] Although PfAOP is supposed to protect *P. falciparum* from hydroperoxides, deletion of the encoding gene was shown to have no effect on the fitness of the asexual blood stages and their susceptibility toward diamide, *tert*-butyl hydroperoxide (*t*BuOOH) or the antimalarial endoperoxide artemisinin.[11] Recombinant PfAOP forms predominantly dimers, has a so-called 1-Cys mechanism because it requires only one cysteine residue for catalysis, and has become a model enzyme for glutathione/glutaredoxin-dependent peroxiredoxins.[12–15] Reduced PfAOP reacts with a hydroperoxide or peroxynitrite, yielding a sulfenic acid enzyme species.[12,14] Reduced glutathione (GSH) and the glutaredoxin PfGrx are probably the physiological reductants of cytosolic PfAOP in accordance with high peroxidase activities in reconstituted hydroperoxidase assays *in vitro*.[12,13] While GSH is the first reducing agent for the sulfenic acid species of PfAOP, PfGrx deglutathionylates PfAOP and therefore acts as the second reducing agent.[12,13] Even though GSH is also present in the apicoplast, the exact reduction mechanism in this organelle remains unknown. Using yeast as a cellular test tube, H_2O_2-dependent oxidation of heterologous PfAOP in the mitochondrial matrix was shown to directly or indirectly result in the formation of glutathione disulfide (GSSG).[15] Previous analyses revealed that the active site residue C117 of PfAOP can be glutathionylated *in vitro* and in *Escherichia coli*, yielding a mixed PfAOP-SSG disulfide.[12] Furthermore, kinetic measurements with recombinant wild-type and mutant PfAOP, including the gain-of-function mutant $PfAOP^{L109M}$, suggested that conformational changes and the first reduction of oxidized PfAOP by GSH are rate limiting for catalysis.[12,13] However, while the oxidation of PfAOP has been characterized for different substrates and mutants *in vitro* and in yeast,[14] the isolated reduction of PfAOP has not been studied to date.

Here, we qualitatively reconstituted and monitored the catalytic cycle of PfAOP *in vitro*. Furthermore, using stopped-flow measurements, we quantified the second-order rate constant and estimated the activation energy and thermodynamic activation parameters $\Delta H^{\ddagger}$, $\Delta S^{\ddagger}$, and $\Delta G^{\ddagger}$ for the rapid GSH-dependent reduction of oxidized PfAOP, thus providing insights into the reactivity of its sulfenic acid and the transition state of the first reduction step of the catalytic cycle of peroxiredoxins.

2 | RESULTS

2.1 | Hydroperoxide- and glutaredoxin-dependent reversible glutathionylation of PfAOP

To qualitatively study the proposed hydroperoxidase mechanism for PfAOP (Figure 1a), we reconstituted the reaction with recombinant proteins and monitored it by western blot analyses and gel mobility shift assays (Figure 1b–d). Treatment of reduced wild-type enzyme ($PfAOP^{WT}$) with 1 equiv of *t*BuOOH and subsequent addition of 1 equiv of GSH yielded PfAOP-SSG (Figure 1b). PfAOP has two cysteine residues, the peroxidatic residue C117 and the nonessential residue C143.[12,13] Comparative studies with $PfAOP^{C143S}$ and $PfAOP^{C117S}$ revealed a specific glutathionylation of active site residue C117 (Figure 1c). The glutathionlyation of residue C117 was reversed by the addition of reduced $PfGrx^{C32S/C88S}$. This glutaredoxin mutant was used because it is catalytically fully active and has only one cysteine residue so that alternative parallel or subsequent thiol-disulfide exchange reactions cannot occur.[12,16,17] The addition of equimolar amounts of $PfGrx^{C32S/C88S}$ resulted in an almost complete loss of the glutathione signal for $PfAOP^{C143S}$-SSG, while only traces of the mixed disulfide between $PfAOP^{C143S}$ and $PfGrx^{C32S/C88S}$ were formed, suggesting a preferential nucleophilic attack of $PfGrx^{C32S/C88S}$ at the glutathione sulfur atom of $PfAOP^{C143S}$-SSG. Increasing the ratio between $PfGrx^{C32S/C88S}$ and $PfAOP^{C143S}$ to 2:1 also resulted in the loss of the glutathione signal but yielded more mixed disulfide between both proteins (Figure 1c). Since the anti-glutathione antibody did not detect glutathionylated $PfGrx^{C32S/C88S}$, we confirmed the transfer of the glutathione-moiety from PfAOP to the single cysteine residue of $PfGrx^{C32S/C88S}$ by labeling available thiol groups with a 1.24 kDa methyl ether poly(ethylene glycol)$_{24}$ maleimide ($mmPEG_{24}$) (Figure 1d). The thiol group of pure reduced $PfGrx^{C32S/C88S}$ was modified by mmPEG24 and resulted in an altered SDS-PAGE mobility as expected.

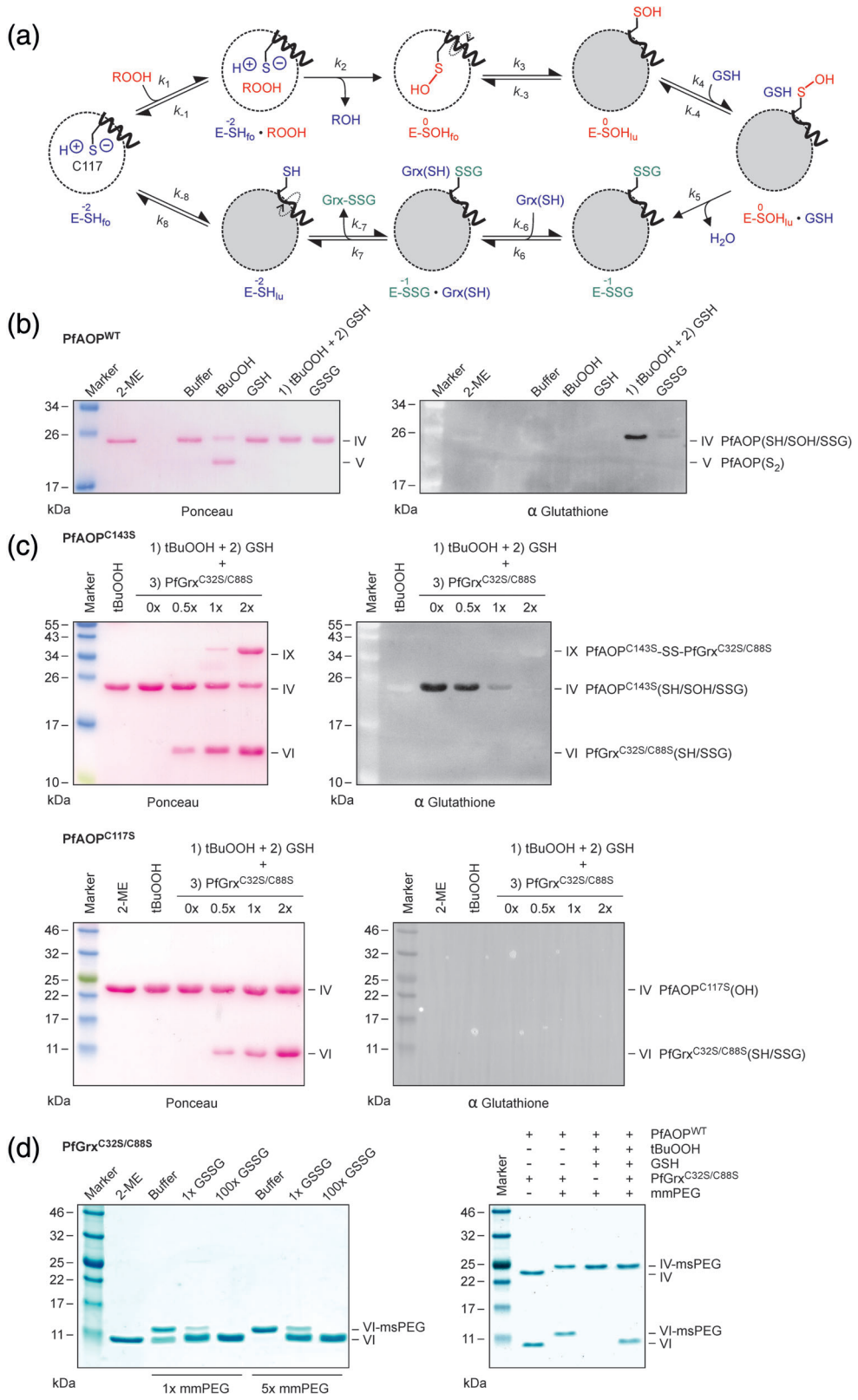

FIGURE 1 Legend on next page.

Incubation of $PfGrx^{C32S/C88S}$ with GSSG or PfAOP-SSG prevented the modification of $PfGrx^{C32S/C88S}$ by $mmPEG_{24}$ in accordance with the formation of $PfGrx^{C32S/C88S}$-SSG. In summary, the reconstituted reaction *in vitro* supports a stepwise oxidation, glutathionylation, and PfGrx-dependent deglutathionylation of residue C117 of PfAOP.

2.2 | Molecular docking of GSH to fully folded PfAOP

Next, we performed molecular docking experiments to address whether GSH can only reduce the sulfenic acid of PfAOP in the locally unfolded protein conformation (Figure 1a) or whether GSH might also attack the C117 sulfur atom of the fully folded protein. A first round of docking experiments for GSH and the fully folded conformation of hyperoxidized $PfAOP^{WT}$ [9] revealed GSH-C117 sulfur–sulfur distances ≥3.8 Å. Since these distances were much longer than the sulfur–sulfur distances of disulfide bonds around 2.0 Å, we optimized the position of the side chain of C117 by rotating it toward the opening of the active site and performed 10 more simulation runs that resulted in 84 different binding modes. Although PfAOP accommodated GSH in a groove on top of the active site pocket, shortest sulfur–sulfur distances were between 3.1 and 3.3 Å (Figure 2a). Binding energies were between −2 and −5 kJ/mol and did not reveal a favorable GSH orientation. Lower binding energies around −20 kJ/mol were actually obtained for the most unfavorable sulfur–sulfur orientations (Figure 2b). In summary, GSH probably cannot get close enough to attack the sulfur atom of C117 in the fully folded enzyme conformation.

2.3 | Direct monitoring of the reaction between GSH and oxidized PfAOP

We previously showed that the oxidation of reduced PfAOP by hydroperoxides can be monitored using stopped-flow fluorescence measurements.[14] Here, we applied the same technique to determine the reaction kinetics of the GSH-dependent first reduction step for recombinant PfAOP (Figure 3). Stopped-flow kinetics with *t*BuOOH-oxidized $PfAOP^{WT}$ in the first syringe and variable concentrations of GSH in the second syringe revealed an altered tryptophan fluorescence after mixing. Higher GSH concentrations did not affect the total change of fluorescence but accelerated the reaction (Figure 3a). Similar kinetics were observed for the *t*BuOOH-oxidized gain-of-function mutant $PfAOP^{L109M}$, although the total change of fluorescence was smaller than for $PfAOP^{WT}$ (Figure 3b) (akin to the smaller change of fluorescence during the oxidation of $PfAOP^{L109M}$ in comparison with $PfAOP^{WT}$ [14]). The altered tryptophan fluorescence of PfAOP was coupled to the reduction of the sulfur atom of C117. This was demonstrated for the inactive mutant $PfAOP^{C117S}$, which lacks the active-site thiol group and, therefore, served as a negative control to exclude unspecific GSH interactions or redox-independent changes of fluorescence (Figure 3c). The stability of *t*BuOOH-oxidized $PfAOP^{WT}$ on ice was analyzed for up to 3 hr. Assays with 5-thio-2-nitrobenzoate (TNB) as a reducing agent (which reacts with neither the sulfinic nor the sulfonic acid species) revealed that 94 ± 4% of $PfAOP^{WT}$ was reversibly oxidized by *t*BuOOH and could be reduced again by TNB. This value did not decrease during the 3-hr incubation. Furthermore, stopped-flow measurements with *t*BuOOH-oxidized PfAOP and GSH also showed no activity loss when the oxidized protein was stored on ice. Thus, *t*BuOOH-oxidized PfAOP was stable enough for subsequent in-depth test series. Although we could not specify whether reversibly *t*BuOOH-oxidized PfAOP comprised just its sulfenic acid species or also a putative cyclic sulfenamide species, we interpret the change of tryptophan fluorescence in accordance with a reaction between GSH and the locally unfolded conformation of the sulfenic acid species. In summary, a redox-dependent reaction between GSH and the oxidized active site of PfAOP can be directly monitored by stopped-flow fluorescence measurements.

FIGURE 1 *In vitro* reconstitution of the catalytic cycle of PfAOP. (a) Proposed catalytic cycle for cytosolic PfAOP (E) with GSH and PfGrx (Grx). Helix α2 of PfAOP adopts two different conformations, a folded conformation (fo) with residue C117 facing the active-site pocket (shown as a dotted circle), and a locally unfolded (lu) conformation with residue C117 facing the protein surface. Oxidized and reduced reactants are shown in red and blue, respectively. The oxidation state of the C117 sulfur atom is indicated for each enzyme species. Enzyme species with an intermediate sulfur oxidation state (−1) are shown in green. (b) GSH glutathionylates recombinant *t*BuOOH-oxidized $PfAOP^{WT}$ as revealed by nonreducing SDS-PAGE, ponceau-staining (shown on the left), and western-blot analysis (shown on the right). A faint glutathionylation signal was also detected following treatment of reduced $PfAOP^{WT}$ with an excess of GSSG. In contrast to correctly folded PfAOP, denatured *t*BuOOH-oxidized $PfAOP^{WT}$ can form the intramolecular disulfide species $PfAOP(S_2)$.[12,13] (c) Reversal of the glutathionylation of *t*BuOOH-oxidized PfAOP depends on active-site residue C117 and the concentration of $PfGrx^{C32S/C88S}$. (d) SDS-PAGE redox mobility shift assays reveal a glutathione transfer from PfAOP to $PfGrx^{C32/88S}$. Treatment of reduced $PfGrx^{C32/88S}$ with GSSG (left side) or with glutathionylated $PfAOP^{WT}$ (right side) prevented an alkylation by $mmPEG_{24}$. The calculated molecular masses of PfAOP and $PfGrx^{C32S/C88S}$ are 22.6 kDa and 13.7 kDa, respectively. Reductions with 2-mercaptoethanol (2-ME) served as controls. Band numbering and identified protein species refer to the literature[12]

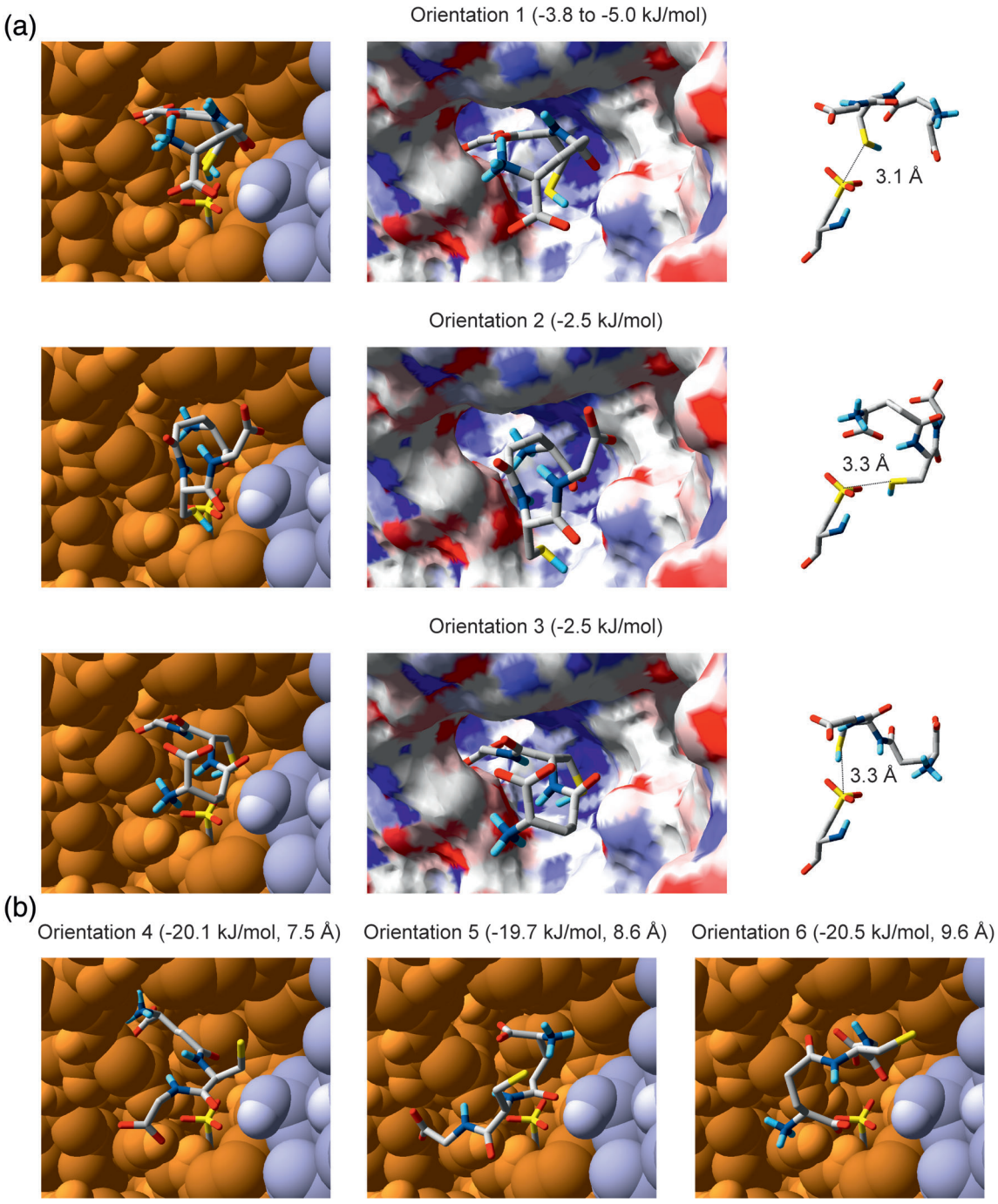

FIGURE 2 Molecular docking of GSH to fully folded PfAOP. (a) Selection of three different GSH binding modes with the shortest sulfur–sulfur distances (orientation 1–3 from top to bottom). The two subunits of PfAOP are shown as space-filling models in orange and lilac on the left. GSH and the sulfonic acid of residue C117 are highlighted as ball-and-stick models. The electrostatic surface potential is depicted in the middle (red −4.0; white 0; blue +4.0). The sulfur–sulfur distances are shown on the right. (b) Selection of three different GSH binding modes with the lowest binding energies (orientation 4–6 from left to right)

2.4 | Kinetic and thermodynamic reaction parameters

We applied the stopped-flow fluorescence measurements to determine the rate constant for the reaction between GSH and *t*BuOOH-oxidized $PfAOP^{WT}$ (assuming that it is predominantly present in its unfolded conformation as a sulfenic acid species) at five different temperatures between 5 and 25°C. The change of fluorescence within the first second after mixing followed first-order kinetics and was fitted accordingly, yielding a k_{obs} value for each GSH concentration. Plotting the k_{obs} values versus the

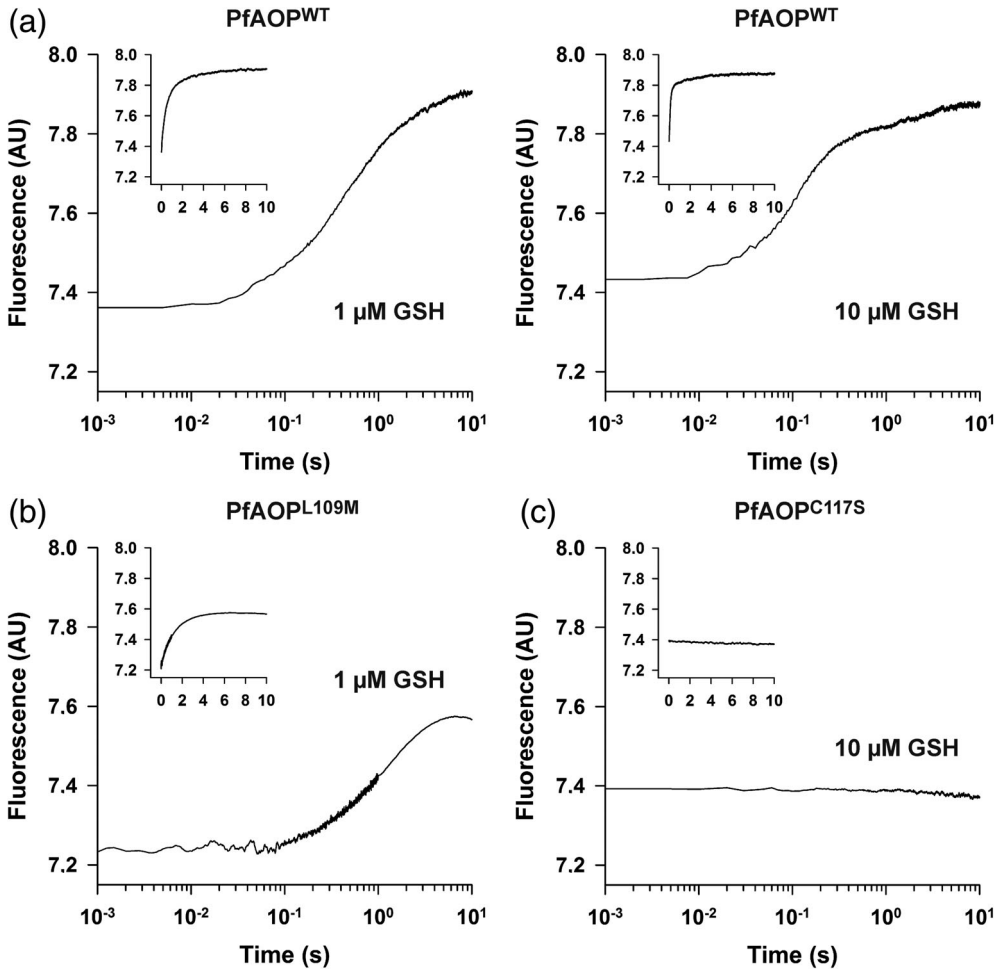

FIGURE 3 Stopped-flow kinetics of the reaction between oxidized PfAOP and GSH. Recombinant reduced PfAOP (2 µM) was oxidized with 1 equiv *t*BuOOH and subsequently mixed 1:1 with variable concentrations of GSH at pH 7.4 and 25°C. Representative kinetic traces are shown for 1 µM PfAOP^{WT} with (a) 1 µM GSH or 10 µM GSH. (b) Reaction kinetics between GSH and the gain-of-function mutant PfAOP^{L109M}. (c) Reaction kinetics between GSH and the redox-inactive negative control PfAOP^{C117S}

GSH concentration revealed a linear correlation, which allowed us to calculate temperature-dependent second-order rate constants k_2 from the slopes of the linear fits (Figure 4a and Table 1). These values of up to $6.1 \times 10^5\ M^{-1}\ s^{-1}$ at 25°C were used to calculate the activation energy and pre-exponential factor A according to Arrhenius theory (Figure 4b) and to estimate the thermodynamic activation parameters $\Delta H^{\ddagger}$ and $\Delta S^{\ddagger}$ according to Eyring–Polanyi theory (Figure 4c and Table 2). Note that these estimates have to be interpreted with care because they are based on macroscopic measurements in aqueous buffers with a postulated transmission coefficient κ and activity coefficients of 1. The activation energy E_a and the enthalpy of activation $\Delta H^{\ddagger}$ were both around 40 kJ/mol. The entropy of activation $\Delta S^{\ddagger}$ was close to zero and, therefore, the Gibbs free energy of activation $\Delta G^{\ddagger}$ was temperature independent (Table 2). In summary, *t*BuOOH-oxidized PfAOP^{WT} rapidly and directly reacts with GSH with a second-order rate constant of $6.1 \times 10^5\ M^{-1}\ s^{-1}$ at 25°C, E_a and $\Delta H^{\ddagger}$ values around 40 kJ/mol, and a $\Delta S^{\ddagger}$ value close to zero, resulting in a temperature-independent $\Delta G^{\ddagger}$ value of 40 kJ/mol.

2.5 | Comparison with the gain-of-function mutant PfAOP^{L109M}

Point mutations at the bottom of the active site were shown to affect the enzyme kinetic parameters of PfAOP. While PfAOP^{WT} and PfAOP^{L109M} had very similar $k_{cat}{}^{app}/K_m{}^{app}$ values and second-order rate constants with hydroperoxide substrates,[13,14] $k_{cat}{}^{app}/K_m{}^{app}$ values of PfAOP^{WT} with GSH from steady-state measurements were more than one order of magnitude smaller than for the gain-of-function mutant PfAOP^{L109M}.[13] To address a potential effect of the L109M mutation on the direct reaction between *t*BuOOH-oxidized PfAOP^{L109M} and GSH, we determined the k_{obs} values and compared the second-order rate constants and thermodynamic activation parameters of PfAOP^{L109M} with the values and parameters of PfAOP^{WT} (Figure 4d–f and Tables 1 and 2). The second-order rate constants and values for E_a, A, $\Delta H^{\ddagger}$, $\Delta S^{\ddagger}$, and $\Delta G^{\ddagger}$ were extremely similar between both data sets. Minor changes of $\Delta S^{\ddagger}$ still had no effect on the temperature-independent $\Delta G^{\ddagger}$ value. In summary, the kinetics and thermodynamic activation parameters for the GSH-dependent reduction of *t*BuOOH-oxidized

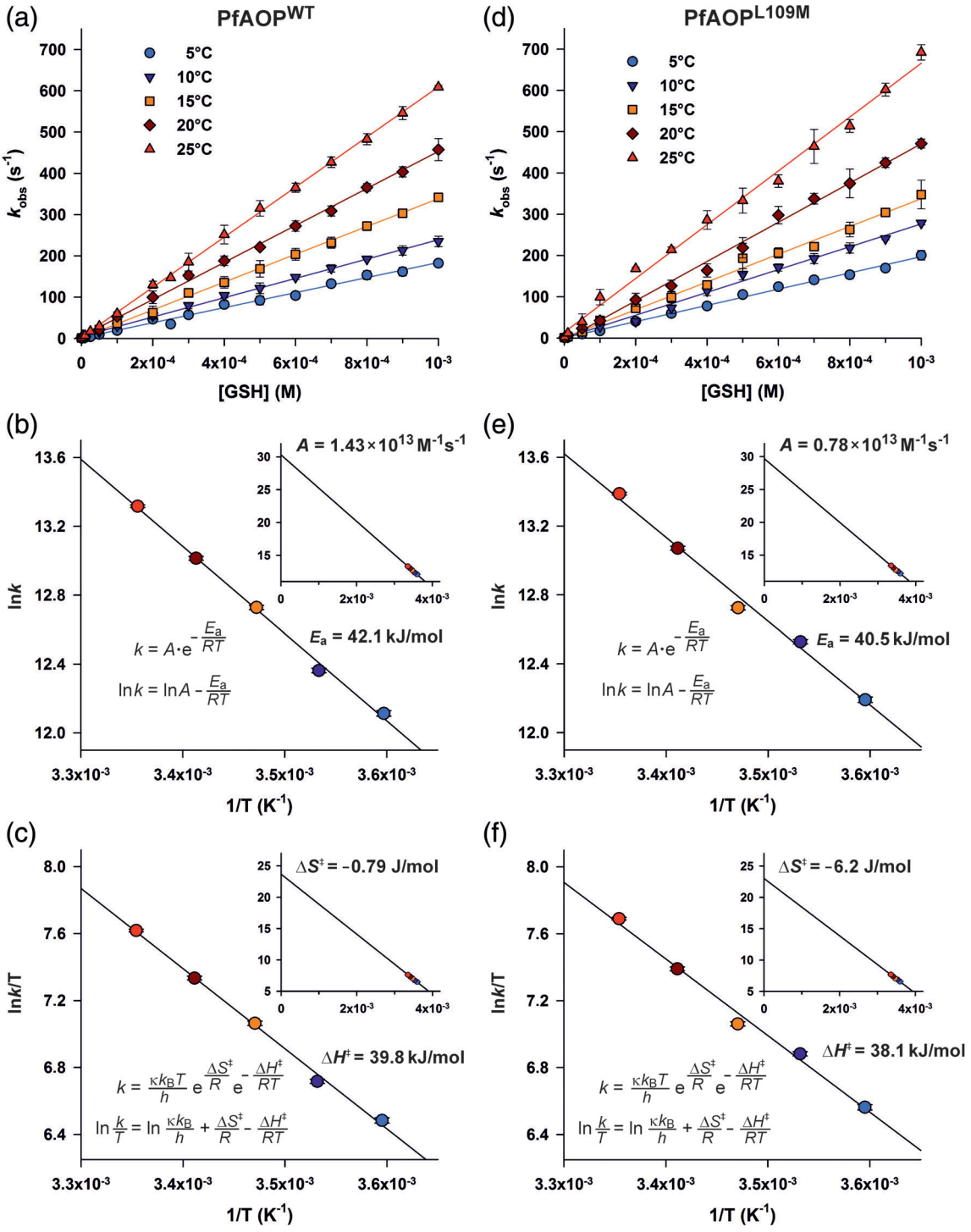

FIGURE 4 Arrhenius and Eyring–Polanyi plots for the reaction between oxidized PfAOP and GSH. (a) Temperature-dependency of the k_{obs} values for the reaction between variable concentrations of GSH and 1 μM PfAOP^{WT} that was pre-oxidized with 1 equiv *t*BuOOH. The data sets at the indicated temperatures were fitted by linear regression and the slopes yielded the second-order rate constants k_2 that are listed in Table 1. (b) The temperature-dependent rate constants from Table 1 were plotted according to the Arrhenius equation. Following linear regression analysis, the pre-exponential factor A and the activation energy E_a were calculated from the *y*-axis intercept and the slope, respectively. (c) The rate constants from Table 1 were also plotted according to Eyring–Polanyi theory to estimate the thermodynamic activation parameters $\Delta H^{\ddagger}$ and $\Delta S^{\ddagger}$. The value for $\Delta S^{\ddagger}$ was calculated with a transmission coefficient $\kappa = 1$. $\Delta S^{\ddagger}$ increases to +5.0 J/mol for $\kappa = 0.5$. (d–f) Analogous analyses for the reaction between 1 μM oxidized PfAOP^{L109M} and GSH. Data in panels (a) and (d) were obtained from three or four independent biological replicates

PfAOP^{L109M} and PfAOP^{WT} do not indicate significant differences between both enzymes and are in accordance with identical mechanisms. The most likely explanation is that both enzymes already adopted the locally unfolded conformation when they were mixed with GSH.

3 | DISCUSSION

The substrate specificity for selected reducing agents remains one of the unresolved topics in peroxiredoxin catalysis. In contrast to 2-Cys peroxiredoxins, the sulfenic acid of 1-Cys peroxiredoxins cannot react with a resolving cysteine and could, therefore, be exposed to a variety of physiological thiols. If and how 1-Cys peroxiredoxins prevent the formation of nonspecific disulfide bonds probably depends on unknown structural and kinetic features. Here, we reconstituted the catalytic cycle for the model enzyme PfAOP and confirmed a stepwise oxidation, glutathionylation, and PfGrx-dependent deglutathionylation of residue C117. Furthermore, stopped-flow measurements provided detailed insights into the kinetics and transition state of the GSH-dependent first reduction of the oxidized enzyme (Figure 5a). While previous steady-state kinetic measurements showed that the GSH-dependent first reduction of PfAOP is rate limiting *in vitro*, they could not discriminate between (a) conformational changes, including local unfolding of helix α2, and (b) the reduction of the sulfenic acid.[13] An infinite "true" k_{cat} value for GSH suggested that the enzyme-substrate complex cannot be saturated, and previous kinetic as well as structural analysis of the gain-of-function mutant PfAOP^{L109M} with its much lower K_m^{app} value for GSH already pointed toward local unfolding of PfAOP as the rate-limiting step during the catalytic cycle.[12,13] Here, we provide four more arguments to support this model. The following interpretations are based on the assumption that *t*BuOOH-oxidized enzyme was present in its sulfenic acid state in accordance with the generally accepted catalytic cycle of peroxiredoxins[2,5,7] and the fact that protein sulfenic acids, for example, in bovine Prx6, can be stable for several minutes or even hours in the absence of thiols or peroxides.[18–20] (a) Docking analyses argue against a direct reaction between GSH and residue C117 of the fully folded conformation of PfAOP. Thus, assuming a similar structure of fully folded PfAOP in its sulfenic and sulfonic acid state,[9] helix α2 has to partially unfold for the reaction to occur. (b) While bulky TNB was shown to react with bovine Prx6 only in the presence of the detergent sodium dodecyl sulfate (SDS), which is indicative for a buried sulfenic acid, oxidized PfAOP readily reacted with TNB in the absence of SDS in accordance with an accessible sulfenic acid that is exposed in the locally unfolded conformation. (c) The GSH-dependent k_{cat}^{app}/K_m^{app} values of PfAOP^{L109M} from steady-state kinetic measurements were roughly 10 times higher than the values for PfAOP^{WT},[13] whereas the stopped-flow second-order rate constants for the reaction between GSH and *t*BuOOH-oxidized PfAOP^{WT} or PfAOP^{L109M} were almost identical (Table 1). In accordance with the kinetics for PfAOP^{WT} and PfAOP^{L109M}, one would expect that residue 109 at the bottom of the active site can affect the stability of the fully folded conformation, and, therefore, influence the K_m^{app} value, but the residue should not affect the reactivity of the sulfenic acid in the locally unfolded protein conformation. (d) The stopped-flow second-order rate constants for the GSH-dependent reduction of *t*BuOOH-oxidized PfAOP^{WT} and PfAOP^{L109M} at pH 7.4 and 25°C were one to three orders of magnitude higher than the k_{cat}^{app}/K_m^{app} values from the biphasic GSH-dependent steady-state kinetics at pH 8.0 and 25°C (Figure 5a).[12,13] Thus, the reaction between the sulfenic acid and GSH is too fast to be rate limiting for this part of the catalytic cycle. In summary, PfAOP first has to undergo a slow conformational change so that the sulfenic acid can rapidly react with GSH (Figure 5a). On the

TABLE 1 Temperature-dependent second-order rate constants from Figure 4 for the reaction between oxidized PfAOP and GSH

	PfAOP^{WT}	PfAOP^{L109M}
T (°C)	k_2 (mM^{-1} s^{-1})	k_2 (mM^{-1} s^{-1})
5	182 ± 3	197 ± 3
10	234 ± 3	276 ± 5
15	337 ± 4	336 ± 7
20	449 ± 5	475 ± 8
25	607 ± 5	652 ± 11
37[a]	1,161	1,189

[a]Calculated from data in Figure 4.

TABLE 2 Activation energy and thermodynamic activation parameters from Figure 4 for the reaction between oxidized PfAOP and GSH

	E_a	A	$\Delta H^{\ddagger}$	$\Delta S^{\ddagger}$	$\Delta G^{\ddagger}_{@25°C/37°C}$
T (°C)	(kJ/mol)	(M/s)	(kJ/mol)	(kJ/mol)	(kJ/mol)
PfAOP^{WT}	42.2	1.4×10^{13}	39.8	-0.8×10^{-3}	40.0/40.0
PfAOP^{L109M}	40.5	7.8×10^{12}	38.1	-6.2×10^{-3}	39.9/40.0

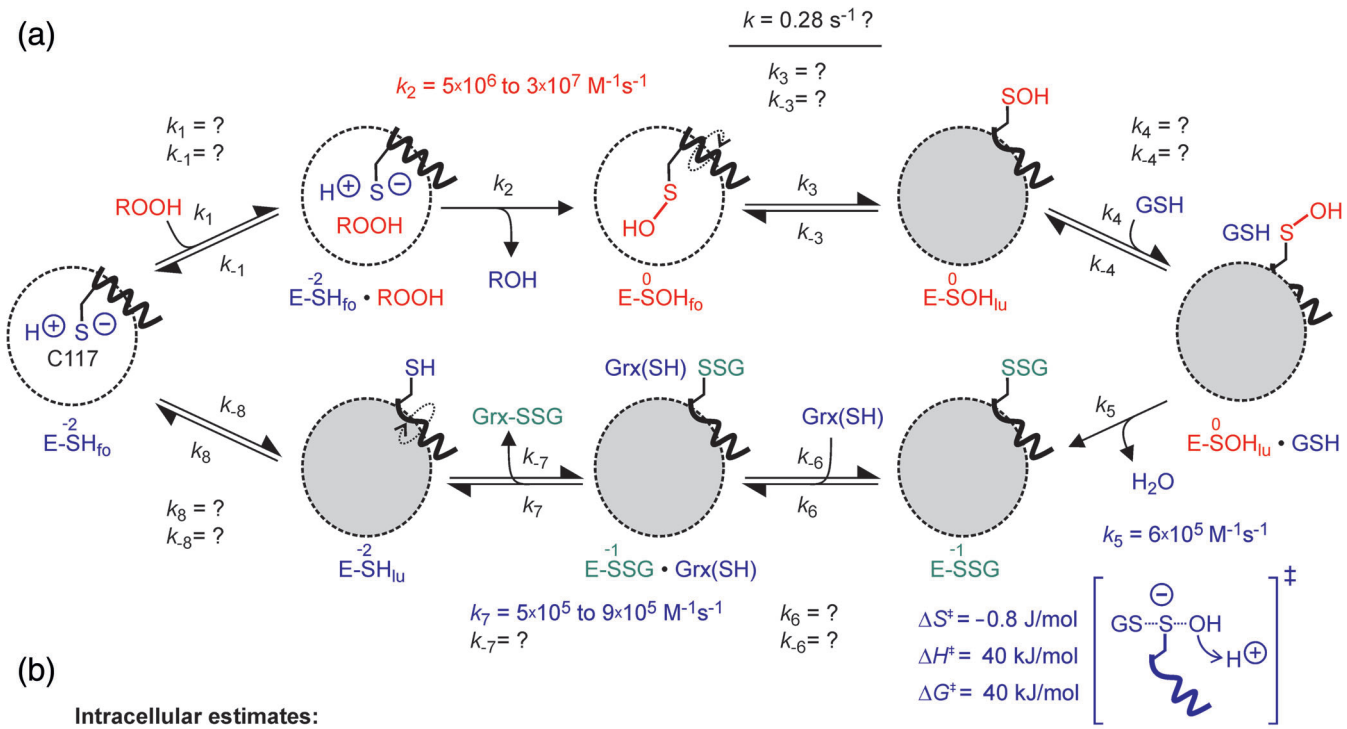

(b)

Intracellular estimates:

$$v_{ox@1\ nM\ ROOH} = \frac{-d[ROOH]}{dt} = k_{2(low)}[ROOH][E\text{-}SH_{fo}] = 5\times10^{6}\ M^{-1}s^{-1} \cdot 10^{-9}\ M \cdot [E\text{-}SH_{fo}] = 5\times10^{-3}\ s^{-1} \cdot [E\text{-}SH_{fo}]$$

$$v_{ox@1\ \mu M\ ROOH} = \frac{-d[ROOH]}{dt} = k_{2(high)}[ROOH][E\text{-}SH_{fo}] = 3\times10^{7}\ M^{-1}s^{-1} \cdot 10^{-6}\ M \cdot [E\text{-}SH_{fo}] = 30\ s^{-1} \cdot [E\text{-}SH_{fo}]$$

$$v_{red@1\ mM\ GSH} = \frac{-d[GSH]}{dt} = k_{5}[GSH][E\text{-}SOH_{lu}] = 6\times10^{5}\ M^{-1}s^{-1} \cdot 10^{-3}\ M \cdot [E\text{-}SOH_{lu}] = 6\times10^{2}\ s^{-1} \cdot [E\text{-}SOH_{lu}]$$

$$v_{red@10\ mM\ GSH} = \frac{-d[GSH]}{dt} = k_{5}[GSH][E\text{-}SOH_{lu}] = 6\times10^{5}\ M^{-1}s^{-1} \cdot 10^{-2}\ M \cdot [E\text{-}SOH_{lu}] = 6\times10^{3}\ s^{-1} \cdot [E\text{-}SOH_{lu}]$$

$$\frac{v_{red(low)}}{v_{ox(high)}} = \frac{6\times10^{2}\ s^{-1} \cdot [E\text{-}SOH_{lu}]}{30\ s^{-1} \cdot [E\text{-}SH_{fo}]} = 20 \cdot \frac{[E\text{-}SOH_{lu}]}{[E\text{-}SH_{fo}]} \qquad \frac{v_{red(high)}}{v_{ox(low)}} = \frac{6\times10^{3}\ s^{-1} \cdot [E\text{-}SOH_{lu}]}{5\times10^{-3}\ s^{-1} \cdot [E\text{-}SH_{fo}]} \approx 10^{6} \cdot \frac{[E\text{-}SOH_{lu}]}{[E\text{-}SH_{fo}]}$$

***In vitro* estimates:**

$$v_{ox@100\ \mu M\ ROOH} = \frac{-d[ROOH]}{dt} = k_{2(low)}[ROOH][E\text{-}SH_{fo}] = 5\times10^{6}\ M^{-1}s^{-1} \cdot 10^{-4}\ M \cdot [E\text{-}SH_{fo}] = 5\times10^{2}\ s^{-1} \cdot [E\text{-}SH_{fo}]$$

$$v_{ox@100\ \mu M\ ROOH} = \frac{-d[ROOH]}{dt} = k_{2(high)}[ROOH][E\text{-}SH_{fo}] = 3\times10^{7}\ M^{-1}s^{-1} \cdot 10^{-4}\ M \cdot [E\text{-}SH_{fo}] = 3\times10^{3}\ s^{-1} \cdot [E\text{-}SH_{fo}]$$

$$v_{red@1\ mM\ GSH} = \frac{-d[GSH]}{dt} = k_{5}[GSH][E\text{-}SOH_{lu}] = 6\times10^{5}\ M^{-1}s^{-1} \cdot 10^{-3}\ M \cdot [E\text{-}SOH_{lu}] = 6\times10^{2}\ s^{-1} \cdot [E\text{-}SOH_{lu}]$$

$$v_{red@10\ mM\ GSH} = \frac{-d[GSH]}{dt} = k_{5}[GSH][E\text{-}SOH_{lu}] = 6\times10^{5}\ M^{-1}s^{-1} \cdot 10^{-2}\ M \cdot [E\text{-}SOH_{lu}] = 6\times10^{3}\ s^{-1} \cdot [E\text{-}SOH_{lu}]$$

$$\frac{v_{red(low)}}{v_{ox(high)}} = \frac{6\times10^{2}\ s^{-1} \cdot [E\text{-}SOH_{lu}]}{3\times10^{3}\ s^{-1} \cdot [E\text{-}SH_{fo}]} = 0.2 \cdot \frac{[E\text{-}SOH_{lu}]}{[E\text{-}SH_{fo}]} \qquad \frac{v_{red(high)}}{v_{ox(low)}} = \frac{6\times10^{3}\ s^{-1} \cdot [E\text{-}SOH_{lu}]}{5\times10^{2}\ s^{-1} \cdot [E\text{-}SH_{fo}]} = 12 \cdot \frac{[E\text{-}SOH_{lu}]}{[E\text{-}SH_{fo}]}$$

FIGURE 5 Updated model and quantitative assessment of the catalytic cycle of PfAOP. (a) Assignment of measured rate constants. Values for k_2 and a combination of k_3 and k_{-3} are from stopped-flow measurements at pH 7.4 and 25°C from the literature.[14] Values for k_7 are from k_{cat}^{app}/K_m^{app} values from steady-state measurements at pH 8.0 and 25°C from refs. 12,13. (b) Estimated reaction velocities for the hydroperoxide-dependent oxidation (v_{ox}) and GSH-dependent first reduction (v_{red}) of PfAOP based on the values from panel (a) and substrate concentrations *in vivo* and *in vitro*

one hand, this explains why glutaredoxin, plasmoredoxin, and thioredoxin could also transfer electrons to oxidized PfAOP *in vitro* (Figure 1c),[12,21] or why oxidized PfAOP was efficiently reduced by fused roGFP2 in yeast.[14] On the other hand, this raises once again the question if and how 1-Cys peroxiredoxins prevent the formation of disulfide bonds with other physiological thiols.

Differences in the Gibbs free energy of activation $\Delta G^{\ddagger}$ could explain the versatile thiol chemistry and substrate specificity. However, thermodynamic activation parameters for peroxiredoxin catalysis are scarce. Studies on the alkyl hydroperoxide reductase E from *Mycobacterium tuberculosis* revealed a $\Delta H^{\ddagger}$ value for the reduction of H_2O_2 of 20 kJ/mol and an unfavorable $\Delta S^{\ddagger}$ value of −80 J/mol, resulting in a $\Delta G^{\ddagger}$ value of 44 kJ/mol at 25°C in accordance with a rather moderate second-order rate constant of $8 \times 10^4\ M^{-1}\ s^{-1}$.[22] The $\Delta G^{\ddagger}$ value of 40 kJ/mol for the GSH-dependent first reduction of PfAOP is temperature independent and smaller in accordance with higher second-order rate constants (Tables 1 and 2). First-order rate constants for the disulfide bond formation in different 2-Cys peroxiredoxins were shown to differ by two orders of magnitude.[23,24] Furthermore, reported second-order rate constants for the reaction between protein or low-molecular-weight sulfenic acids and low-molecular-weight thiols such as cysteine or GSH were shown to differ by at least five orders of magnitude.[18,19,25] Our second-order rate constant of $6 \times 10^5\ M^{-1}\ s^{-1}$ for the reaction between oxidized PfAOP and GSH is on the upper limit of the reported values. This is not a general feature of peroxiredoxins. For example, the reduction of peroxiredoxin 6-type enzymes usually occurs very slowly in the presence of GSH or other common reducing agents.[7,21,26–30] Deciphering the underlying cause for the different reactivity will require much more structural and kinetic information. We therefore suggest to compare not only the structures but also the rate constants and thermodynamic activation parameters of alternative combinations of 1-Cys peroxiredoxins and thiol substrates to better understand this part of the reaction cycle.

Is the hydroperoxide-dependent oxidation, the GSH-dependent first reduction, or the Grx-dependent second reduction of PfAOP faster at physiological substrate concentrations? Rate constants k_2 for the reaction between reduced PfAOP and hydroperoxides at pH 7.4 and 25°C were between $5 \times 10^6\ M^{-1}\ s^{-1}$ and $3 \times 10^7\ M^{-1}\ s^{-1}$,[14] which is one or two orders of magnitude higher than the value of k_5 for GSH (Figure 5a). If we (a) take into account that the enzyme has ping-pong kinetics with separated half-reactions,[12,13] (b) use estimated intracellular hydroperoxide concentrations between 1 and 10^3 nM as well as GSH concentrations between 1 and 10 mM,[31] and (c) assume similar steady-state concentrations of oxidized and reduced PfAOP (which are unknown variables that remain to be determined), the rate constants translate into an estimated reaction velocity ratio ν_{red}:ν_{ox} between 20 and 10^6 (Figure 5b). Thus, at physiological substrate concentrations, the GSH-dependent first reduction of the locally unfolded oxidized enzyme could be faster than the hydroperoxide-dependent oxidation of the fully folded reduced enzyme. A more balanced estimated ν_{red}:ν_{ox} ratio between 0.2 and 12 is obtained using the same numbers except for a hydroperoxide concentration of 100 μM based on *in vitro* experiments.[12,13] The second-order rate constant for the PfGrx-dependent second reduction of cytosolic PfAOP-SSG is probably in the range between $10^5\ M^{-1}\ s^{-1}$ and $10^6\ M^{-1}\ s^{-1}$ in accordance with measured $k_{cat}{}^{app}/K_m{}^{app}$ values for PfAOP[12,13] and PfGrx reaction kinetics with glutathionylated model substrates.[16] Whether the deglutathionylation can become rate limiting under physiological conditions therefore depends on the PfGrx concentration and the steady-state concentrations of the involved enzyme species. What also remains to be analyzed for PfAOP catalysis is (a) the reduction of PfAOP-SSG in the apicoplast, including the identification and characterization of the physiological second reducing agent, and (b) to which degree the macroscopic $k_{cat}{}^{app}/K_m{}^{app}$ values for hydroperoxides and GSH (which are all much smaller than the second-order rate constants from the stopped-flow measurements in Table 1[12–14]) translate into microscopic rate constants that include the rate-limiting conformational changes of PfAOP. Such insights, for example, from stopped-flow circular dichroism measurements, might also explain the biphasic kinetic patterns with GSH from steady-state kinetic measurements[12,13] that were absent in the stopped-flow kinetic measurements (Figure 4).

In conclusion, we generated a reference data set of the thermodynamic activation parameters for the reaction between GSH and a 1-Cys peroxiredoxin 5-type model enzyme with implications for the reactivity and substrate specificity of peroxiredoxin sulfenic acids.

4 | MATERIALS AND METHODS

4.1 | Materials

Recombinant N-terminally $MRGSH_6GS$-tagged $PfAOP^{WT}$, $PfAOP^{C117S}$, $PfAOP^{C143S}$, $PfAOP^{L109M}$, and $PfGrx^{C32S/C88S}$ were produced in *Escherichia coli* strain XL1-Blue and purified by Ni-NTA affinity chromatography as described previously.[12,13,32] Diethylenetriaminepentaacetic acid (DTPA), *t*BuOOH, and 1,4-dithiothreitol (DTT) were

from Sigma Aldrich, the anti-glutathione antibody was from Thermo Fisher Scientific, the goat anti-mouse antibody-HRP conjugate was from Bio-Rad, and $mmPEG_{24}$ (CAS# 88504-24-9) was from Iris Biotech. A 500 mM stock solution of $mmPEG_{24}$ was prepared in DMSO under inert conditions (N_2). All enzymes and reactants were diluted/dissolved in ice-cold assay buffer, containing 100 mM $Na_xH_yPO_4$, 0.1 mM DTPA, pH 7.4.

4.2 | Sample preparation and western blot analysis

Freshly purified $PfAOP^{WT}$, $PfAOP^{C117S}$, $PfAOP^{C143S}$, and $PfGrx^{C32S/C88S}$ were reduced with 5 mM DTT on ice for 30 min. Excess DTT and imidazole were removed on a PD-10 desalting column (Merck), and the reduced proteins were eluted with 3.5 ml ice-cold assay buffer. PfAOP concentrations of the eluates, which were usually around 0.2 mM, were determined spectrophotometrically using a molar extinction coefficient $\varepsilon_{280\,nm}$ of 21.43 mM/cm (as calculated at http://web.expasy.org/protparam). The reduced proteins were diluted with assay buffer to a final concentration of 20 μM and incubated for 30 min on ice with either buffer, 50 equiv of GSSG, 1 equiv of *t*BuOOH, or 1 equiv of GSH. Aliquots of *t*BuOOH-oxidized PfAOP were subsequently incubated with 1 equiv of GSH for 30 min on ice, and, if indicated, for another 30 min with 0–2 equiv of $PfGrx^{C32S/C88S}$. Subsequent redox reactions were blocked by the addition of 20 mM iodoacetamide in Laemmli buffer. The protein samples were heated for 5 min at 95°C, separated by nonreducing SDS-PAGE, blotted onto PVDF membranes, and stained with ponceau. Destained membranes were subsequently probed with a commercial monoclonal mouse anti-glutathione antibody (diluted 1:1000) and a commercial goat anti-mouse antibody-HRP conjugate.

4.3 | Electrophoretic mobility shift assays

Reduced 20 μM $PfGrx^{C32S/C88S}$ was incubated with either buffer or 1 or 100 equiv of GSSG for 30 min on ice. Reduced 20 μM $PfAOP^{WT}$ was obtained as outlined above. The protein was either incubated with buffer or was oxidized, glutathionylated, and deglutathionylated by the stepwise addition of 1 equiv of *t*BuOOH, 1 equiv of GSH, and 1 equiv of $PfGrx^{C32S/C88S}$ as described above. Subsequent redox reactions were blocked by the addition of the indicated concentrations of $mmPEG_{24}$ in Laemmli buffer. The protein samples were heated for 5 min at 95°C and separated by nonreducing SDS-PAGE.

4.4 | Stopped-flow kinetic measurements

$PfAOP^{WT}$ or $PfAOP^{L109M}$ was freshly purified, reduced, and desalted in assay buffer as described above. $PfAOP^{WT}$ or $PfAOP^{L109M}$ were subsequently diluted to 2.0 μM with assay buffer containing 1 equiv of *t*BuOOH and incubated on ice for 30 min. Stopped-flow measurements were performed either at 25°C or at the indicated temperature in a thermostatted SX-20 spectrofluorometer (Applied Photophysics) with 2.0 μM oxidized enzyme in the first syringe and 2.0 μM to 2.0 mM GSH in assay buffer in the second syringe. The change of fluorescence was measured for 10 s after mixing (total emission at an excitation wavelength of 295 nm with a slit width of 2 mm). The values of three consecutive measurements were averaged and fitted by single exponential regression using the Pro-Data SX software (Applied Photophysics). Rate constants k_{obs} were plotted against the substrate concentration in SigmaPlot 13.0 to obtain second-order rate constants from the slopes of the linear fits. The second-order rate constants were subsequently plotted and fitted according to Arrhenius and Eyring–Polanyi theory.

4.5 | TNB oxidation assay

To assess the stability of *t*BuOOH-oxidized $PfAOP^{WT}$, the concentration of reversibly oxidized enzyme was quantified with TNB as described previously.[20,33] A solution with 50 μM TNB was freshly generated by adding 25 μM DTT to 25.6 μM 5,5′-dithiobis(2-nitrobenzoic acid) in assay buffer. Samples with 20 μM freshly *t*BuOOH-oxidized $PfAOP^{WT}$ were incubated for 0, 30, 60, 120, or 180 min on ice and were subsequently mixed with an equal volume of the 50 μM TNB solution. The reduction of oxidized $PfAOP^{WT}$ by TNB was monitored at 412 nm (ε = 13.6 mM/cm) using a thermostated Jasco V-550 UV/vis spectrophotometer at 25°C.

4.6 | Molecular docking

A structure data file (SDF) for GSH was downloaded from PubChem (https://pubchem.ncbi.nlm.nih.gov/compound/124886) and converted in PyMol v2.5.2 into a PDB file. The PDB file for GSH was opened in AutoDockTools v1.5.6 (https://ccsb.scripps.edu/mgltools/downloads) to define flexible bonds and to alter the protonation state in accordance with a physiological pH. The PDB file for $PfAOP^{WT}$ (entry 1XIY[9]) was also opened in AutoDockTools v1.5.6 to remove all water molecules, add

hydrogen atoms, and calculate Kollmann-charges. The files were stored in PDBQT format and docking was performed with AutoDock Vina v1.1.2.[34,35] The grid was centered around the sulfur atom of C117 of PfAOP, and the grid size was set to 15 in each dimension. The exhaustiveness was set to 24. Binding modes with a negative binding affinity were visualized in PyMol (https://pymol.org/2) and Swiss PDB viewer v4.1.0[36] to determine sulfur–sulfur distances. The electrostatic surface potential of PfAOP was computed with Swiss PDB viewer using atomic partial charges with a dielectric constant of 78.54 for the solvent (Poisson–Boltzmann computation with a dielectric constant of 4 for the protein and a solvent ionic strength of 0.1 M). For a second round of experiments, the side chain of C117 was rotated toward the opening of the active site using the Swiss PDB viewer to further optimize and shorten the sulfur–sulfur distance. The file was converted again to PDBQT format and used for docking as described above.

ACKNOWLEDGMENTS

This work was funded by the Deutsche Forschungsgemeinschaft (DFG) in the frame of the priority program SPP 1710 (grant DE 1431/8-2). The authors thank Fabian Geissel for help with the stopped-flow measurements and Christoph van Wüllen for discussions regarding the pre-exponential factor *A*. Open access funding enabled and organized by Projekt DEAL.

AUTHOR CONTRIBUTIONS

Robin Schumann: Data curation (equal); formal analysis (equal); investigation (equal); methodology (lead). **Lukas Lang:** Data curation (equal); formal analysis (equal); investigation (equal); methodology (lead); writing – review and editing (supporting). **Marcel Deponte:** Conceptualization (lead); data curation (supporting); formal analysis (supporting); funding acquisition (lead); project administration (lead); resources (lead); supervision (lead); visualization (lead); writing – original draft (lead); writing – review and editing (lead).

ORCID

Marcel Deponte https://orcid.org/0000-0003-2141-917X

REFERENCES

1. Rhee SG, Kil IS. Multiple functions and regulation of mammalian peroxiredoxins. Annu Rev Biochem. 2017;86:749–775.
2. Perkins A, Nelson KJ, Parsonage D, Poole LB, Karplus PA. Peroxiredoxins: Guardians against oxidative stress and modulators of peroxide signaling. Trends Biochem Sci. 2015;40:435–445.
3. Deponte M, Lillig CH. Enzymatic control of cysteinyl thiol switches in proteins. Biol Chem. 2015;396:401–413.
4. Stocker S, Van Laer K, Mijuskovic A, Dick TP. The conundrum of hydrogen peroxide signaling and the emerging role of peroxiredoxins as redox relay hubs. Antioxid Redox Signal. 2018;28:558–573.
5. Hall A, Nelson K, Poole LB, Karplus PA. Structure-based insights into the catalytic power and conformational dexterity of peroxiredoxins. Antioxid Redox Signal. 2011;15:795–815.
6. Soito L, Williamson C, Knutson ST, Fetrow JS, Poole LB, Nelson KJ. PREX: PeroxiRedoxin classification indEX, a database of subfamily assignments across the diverse peroxiredoxin family. Nucleic Acids Res. 2011;39:D332–D337.
7. Deponte M. Glutathione catalysis and the reaction mechanisms of glutathione-dependent enzymes. Biochim Biophys Acta. 2013;1830:3217–3266.
8. Jortzik E, Becker K. Thioredoxin and glutathione systems in *Plasmodium falciparum*. Int J Med Microbiol. 2012;302:187–194.
9. Sarma GN, Nickel C, Rahlfs S, Fischer M, Becker K, Karplus PA. Crystal structure of a novel *Plasmodium falciparum* 1-Cys peroxiredoxin. J Mol Biol. 2005;346:1021–1034.
10. Djuika CF, Huerta-Cepas J, Przyborski JM, et al. Prokaryotic ancestry and gene fusion of a dual localized peroxiredoxin in malaria parasites. Microb Cell. 2015;2:5–13.
11. Djuika CF, Staudacher V, Sanchez CP, Lanzer M, Deponte M. Knockout of the peroxiredoxin 5 homologue PFAOP does not affect the artemisinin susceptibility of *Plasmodium falciparum*. Sci Rep. 2017;7:4410.
12. Djuika CF, Fiedler S, Schnolzer M, Sanchez C, Lanzer M, Deponte M. Plasmodium falciparum antioxidant protein as a model enzyme for a special class of glutaredoxin/glutathione-dependent peroxiredoxins. Biochim Biophys Acta. 2013;1830:4073–4090.
13. Staudacher V, Djuika CF, Koduka J, et al. *Plasmodium falciparum* antioxidant protein reveals a novel mechanism for balancing turnover and inactivation of peroxiredoxins. Free Radic Biol Med. 2015;85:228–236.
14. Staudacher V, Trujillo M, Diederichs T, et al. Redox-sensitive GFP fusions for monitoring the catalytic mechanism and inactivation of peroxiredoxins in living cells. Redox Biol. 2018;14:549–556.
15. Calabrese G, Peker E, Amponsah PS, et al. Hyperoxidation of mitochondrial peroxiredoxin limits H2 O2 -induced cell death in yeast. EMBO J. 2019;38:e101552.
16. Begas P, Liedgens L, Moseler A, Meyer AJ, Deponte M. Glutaredoxin catalysis requires two distinct glutathione interaction sites. Nat Commun. 2017;8:14835.
17. Begas P, Staudacher V, Deponte M. Systematic re-evaluation of the bis(2-hydroxyethyl)disulfide (HEDS) assay reveals an alternative mechanism and activity of glutaredoxins. Chem Sci. 2015;6:3788–3796.
18. Gupta V, Carroll KS. Sulfenic acid chemistry, detection and cellular lifetime. Biochim Biophys Acta. 2014;1840:847–875.
19. Turell L, Botti H, Carballal S, et al. Reactivity of sulfenic acid in human serum albumin. Biochemistry. 2008;47:358–367.
20. Peshenko IV, Shichi H. Oxidation of active center cysteine of bovine 1-Cys peroxiredoxin to the cysteine sulfenic acid form by peroxide and peroxynitrite. Free Radic Biol Med. 2001;31:292–303.
21. Nickel C, Rahlfs S, Deponte M, Koncarevic S, Becker K. Thioredoxin networks in the malarial parasite *Plasmodium falciparum*. Antioxid Redox Signal. 2006;8:1227–1239.
22. Zeida A, Reyes AM, Lebrero MC, Radi R, Trujillo M, Estrin DA. The extraordinary catalytic ability of peroxiredoxins: A combined experimental and QM/MM study on

the fast thiol oxidation step. Chem Commun (Camb). 2014;50:10070–10073.
23. Portillo-Ledesma S, Randall LM, Parsonage D, et al. Differential kinetics of two-cysteine peroxiredoxin disulfide formation reveal a novel model for peroxide sensing. Biochemistry. 2018;57:3416–3424.
24. Trujillo M, Clippe A, Manta B, et al. Pre-steady state kinetic characterization of human peroxiredoxin 5: Taking advantage of Trp84 fluorescence increase upon oxidation. Arch Biochem Biophys. 2007;467:95–106.
25. Nagy P, Ashby MT. Reactive sulfur species: Kinetics and mechanisms of the oxidation of cysteine by hypohalous acid to give cysteine sulfenic acid. J Am Chem Soc. 2007;129:14082–14091.
26. Kang SW, Baines IC, Rhee SG. Characterization of a mammalian peroxiredoxin that contains one conserved cysteine. J Biol Chem. 1998;273:6303–6311.
27. Manevich Y, Feinstein SI, Fisher AB. Activation of the antioxidant enzyme 1-CYS peroxiredoxin requires glutathionylation mediated by heterodimerization with pi GST. Proc Natl Acad Sci U S A. 2004;101:3780–3785.
28. Deponte M, Becker K. Biochemical characterization of Toxoplasma gondii 1-Cys peroxiredoxin 2 with mechanistic similarities to typical 2-Cys Prx. Mol Biochem Parasitol. 2005;140:87–96.
29. Loumaye E, Andersen AC, Clippe A, et al. Cloning and characterization of Arenicola marina peroxiredoxin 6, an annelid two-cysteine peroxiredoxin highly homologous to mammalian one-cysteine peroxiredoxins. Free Radic Biol Med. 2008;45:482–493.
30. Feld K, Geissel F, Liedgens L, Schumann R, Specht S, Deponte M. Tyrosine substitution of a conserved active-site histidine residue activates *Plasmodium falciparum* peroxiredoxin 6. Protein Sci. 2019;28:100–110.
31. Deponte M. The incomplete glutathione puzzle: Just guessing at numbers and figures? Antioxid Redox Signal. 2017;27:1130–1161.
32. Urscher M, More SS, Alisch R, Vince R, Deponte M. Tight-binding inhibitors efficiently inactivate both reaction centers of monomeric *Plasmodium falciparum* glyoxalase 1. FEBS J. 2012;279:2568–2578.
33. Poole LB, Claiborne A. The non-flavin redox center of the streptococcal NADH peroxidase. II. Evidence for a stabilized cysteine-sulfenic acid. J Biol Chem. 1989;264:12330–12338.
34. Trott O, Olson AJ. AutoDock Vina: Improving the speed and accuracy of docking with a new scoring function, efficient optimization, and multithreading. J Comput Chem. 2010;31:455–461.
35. Seeliger D, de Groot BL. Ligand docking and binding site analysis with PyMOL and Autodock/Vina. J Comput Aided Mol Des. 2010;24:417–422.
36. Guex N, Peitsch MC. SWISS-MODEL and the Swiss-PdbViewer: An environment for comparative protein modeling. Electrophoresis. 1997;18:2714–2723.

How to cite this article: Schumann R, Lang L, Deponte M. Characterization of the glutathione-dependent reduction of the peroxiredoxin 5 homolog PfAOP from *Plasmodium falciparum*. Protein Science. 2022;31(5):e4290. https://doi.org/10.1002/pro.4290